

# Tuning Turbines in a Tidal Channel

ROSS VENNELL

Ocean Physics Group, Department of Marine Science  
University of Otago, Dunedin 9054, New Zealand, ross.vennell@otago.ac.nz

(Received Tuesday 27<sup>th</sup> July, 2010 12:13 and in revised form ??)

As tidal turbine farms grow they interact with the larger scale flow along a channel by increasing the channel's drag coefficient. This interaction limits a channel's potential to produce power. The tuning of the flow through the turbines and the density of turbines in a channel's cross-section also interacts with the larger scale flow, via the drag coefficient, to determine the power available for production. To maximise turbine efficiency, i.e. the power available per turbine, farms must occupy the largest fraction of a channel's cross-section permitted by navigational and environmental constraints. Maximising power available with these necessarily densely packed farms requires turbines to be tuned for a particular channel and turbine density. The optimal through-flow tuning fraction varies from near 1/3 for small farms occupying a small fraction of the cross-section, to near 1 for large farms occupying most of the cross-section. Consequently tunings are higher than the optimal through-flow tuning of 1/3 for an isolated turbine from classic turbine theory. Large optimally tuned farms can realise most of a channel's potential. Optimal tunings are dependent on the number of turbines per row, the number of rows, as well as channel geometry, background bottom friction coefficient and the tidal forcing.

---

## 1. Introduction

Many possible sites for generating electricity from tidal currents are found in the high flows through narrow channels and straits that connect parts of the ocean with different tidal regimes. It is essential to have a method to assess the potential of a tidal channel to generate power. Early assessment methods were based on the average kinetic energy (KE) flux through the undisturbed channel (see review by Blunden & Bahaj (2007)). Garrett & Cummins (2005) (hereafter GC05) showed that KE flux considerably overestimates a channel's potential because it does not account for the influence the turbines have on the flow. Their simple 1D model showed how extracting power from turbines increases a channel's total drag coefficient, slowing flow along the channel. This interaction of turbines with the flow results in a peak in the power curve, which quantifies a channel's potential to produce power. This paper takes GC05's result to the next level. Whereas they showed how the interaction between the turbines and the macroscopic flow along the channel limits its potential, this work explores how aspects of the internal configuration of a farm, turbine through-flow tuning and density, interact with the larger scale flow and how these aspects determine the maximum power available for production. The work aims to improve understanding of how to scale up single turbines into large tidal energy farms. It may be the first to show that maximising production requires turbines to be tuned for a particular tidal channel.

GC05's estimate of potential assumes that turbines occupy the entire cross-section of a channel. However, to allow for navigation of vessels and marine life along a channel farms

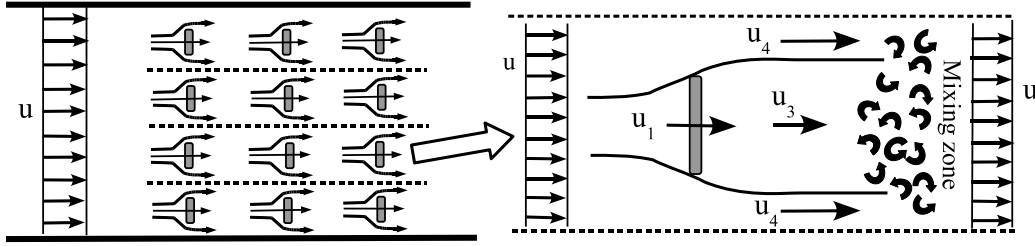


FIGURE 1. A schematic of a turbine farm in a channel with gaps between turbines arranged in rows to form a grid. Adjacent turbines create virtual walls, given by the dashed lines. These walls enhance the flow bypassing the turbines relative to the slower flows through the turbines; so that  $u_4 \geq u > u_1 > u_3$ . Adapted from Garrett & Cummins (2007).

will require gaps between turbines. When there are gaps Garrett & Cummins (2007) (hereafter GC07) showed that mixing of the enhanced flow through the gaps downstream of the turbines with the slower flow passing through the turbines dissipates energy, Fig. 1. As a result of this wake dissipation there is a distinction between a channel's potential, which is the maximum power lost by the flow due to the turbines, and the smaller power available for electricity production.

The GC07 model maximises the power available by tuning the velocity downstream of the turbine,  $u_3$ , to be  $1/3$  of the free stream-flow  $u$ , Fig. 1. This through-flow tuning would typically be done by adjusting the pitch of the turbine's blades. GC07's optimal tuning for a channel did not vary with the fraction of a channel's cross-section taken up by the turbines and was the same as that found by Lanchester (1915) and Betz (1920) for an isolated turbine. In GC07 the farm's drag coefficient is dependent on how the turbines are tuned. GC07's optimal tuning of  $1/3$  is based on the assumption that the free-stream flow is constant, i.e. there is no interaction between the drag coefficient associated with power extraction and the free-stream flow. However, in GC05's model, flow along the channel is not constant, as there is an interaction between power extraction and the free-stream flow along the channel, via the farm's gross drag coefficient. Consequently, the optimally tuned turbines of GC07 cannot be directly combined with the GC05 model (as done briefly in GC07 and Garrett & Cummins (2008) to comment on the desirable number of turbine rows) because the free-stream flow  $u$  is a function of the tuning.

GC07 gives the optimal tuning for a given along-channel flow, whereas the properly combined GC05 and GC07 model developed here gives the optimal tuning for a given headloss between the ends of a tidal channel. This properly combined model may be the first to span the transition from a single isolated turbine generating power from the flow's kinetic energy (the classic Lanchester-Betz turbine) to large farms occupying the whole cross-section generating power from headloss across the farm (GC05). Spanning this transition is made possible by the novel realisation that optimal tunings vary in tidal channels.

This paper uses a deliberately simple idealised model to explore optimal tunings, i.e. the internal configuration of the farm required to maximise power production. The understanding provided by the simplified 1D model used here is critical to those developing 2D and 3D numerical models of the sites of proposed turbine farms and will enable them to more efficiently explore how to optimise their farms.

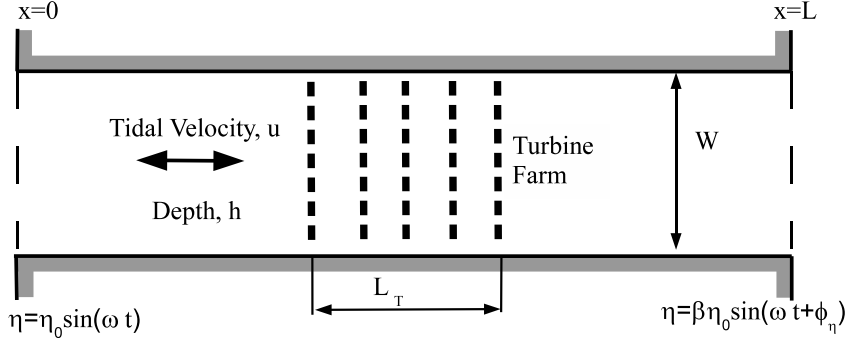


FIGURE 2. Schematic diagram of a turbine farm with a grid of turbines in a narrow channel which connects two large water bodies. Channel has length  $L$ , depth  $h$  and width  $W$ .  $L_T$  is the length of channel occupied by the turbine farm. Flow is forced by differences in water level,  $\eta$ , between the ends.

## 2. Channel Model

GC05's model for turbines in a tidal channel connecting two large water bodies is outlined. Here, for simplicity, only channels with a uniform rectangular cross-section are considered and the effects of a variable cross-section and an exiting jet included in GC05's model will be discussed in a future work. Consider a shallow narrow tidal channel with a uniform rectangular cross-section that connects two large water bodies, Fig. 2. The channel has a turbine farm confined to a short section of the channel, with turbines arranged in a grid. Tidal currents are driven through the channel by the difference in surface elevation between the water bodies and are assumed uniform across the channel. In addition it is assumed that the channel is short enough that velocity does not vary along the channel. Vennell (1998) derived conditions for channels with a range of dynamical balances to be considered short enough to neglect the variation in the transport along a channel. Here the starting point is the 1D shallow water momentum balance for the channel as a whole

$$\rho A_c L \frac{\partial u}{\partial t} = -\rho g A_c (\eta|_{x=L} - \eta|_{x=0}) - \rho C_D W L |u|u - \rho C_T A_c |u|u \quad (2.1)$$

where  $u(t)$  is the along channel velocity,  $\eta$  is the displacement of the water's free surface (assumed small compared to the water depth  $h$ ),  $A_c$  the channel's cross-sectional area,  $L$  the channel's length and  $W$  its width. The first term in (2.1) is the rate of change of momentum of the fluid within the channel, the second is the pressure force due to the water level difference between the ends of the channel, the third is the force due to background bottom friction and the last is the force due to the turbines.  $C_D$  is the drag coefficient for bottom friction and  $C_T$  the farm's gross drag coefficient based on cross-sectional area. For a single forcing frequency,  $\omega$ , the water level difference between the ends can be written in the form  $\Delta \eta_0 \sin(\omega t + \phi_g)$ , where  $\Delta = \sqrt{1 - 2\beta \cos \phi_\eta + \beta^2}$  and  $\phi_g = \tan^{-1}(\beta \sin \phi_\eta / (1 - \beta \cos \phi_\eta))$ ,  $\beta$  is the ratio of the amplitudes of the surface elevation at the ends and  $\phi_\eta$  is the phase lead of the tidal elevation at  $x = L$ , Fig. 2.  $\phi_g$  is the phase of the water level difference between the ends of the channel relative to the surface elevation's phase at  $x = 0$ . With this the governing equation (2.1) becomes

$$\frac{\partial u}{\partial t} = a \sin(\omega t + \phi_g) - \left( \frac{C_D}{h} + \frac{C_T}{L} \right) |u|u \quad (2.2)$$

where  $a = g\eta_0\Delta/L$ . After non-dimensionalising the velocity by  $a/\omega$ , the amplitude of the velocity in the channel with no background friction or turbines, and time by  $1/\omega$  then the governing equation becomes GC05's

$$\frac{\partial u'}{\partial t'} = \sin(t' + \phi_g) - (\lambda_0 + \lambda_T) |u'|u' \quad (2.3)$$

The non-dimensional drag coefficients are  $\lambda_0 = \alpha C_D L/h$  and  $\lambda_T = \alpha C_T$  where  $\alpha = \frac{a}{\omega^2 L}$ . The parameter  $\alpha$  is introduced for conciseness, it has no obvious physical meaning but in combination with the farm's drag coefficient  $\alpha C_T$ . i.e.  $\lambda_T$ , gives the relative importance of drag on the farm and the tidal forcing. Similarly, the parameter  $\alpha C_D L/h$ . i.e.  $\lambda_0$ , gives the relative importance of background bottom friction and the tidal forcing. In  $\lambda_0$  the geometric ratio  $L/h$  occurs because the bottom friction drag coefficient is based on the channel's horizontal area, whereas the farm's drag coefficient is based on the channel's cross-sectional area.

Non-dimensionally the power lost by the flow due to the turbines averaged over a tidal cycle relative to a channel's potential can be expressed as

$$\frac{\overline{P}_{lost}}{\overline{P}_{max}} = \frac{\lambda_T \overline{|u'(t', \lambda_0 + \lambda_T)|^3}}{\lambda_{Tpeak} \overline{|u'(t', \lambda_0 + \lambda_{Tpeak})|^3}} \quad (2.4)$$

where the over bar indicates an average over a tidal cycle.  $\overline{P}_{max}$  is the maximum power that can be extracted, i.e. the channel's potential, given by the average power lost by flow at the peak in the power curve, Fig. 3a.  $\lambda_{Tpeak}$  is the farm's gross drag coefficient at the peak in the power lost curve. It will be shown later that  $\lambda_{Tpeak}$  (3.1) depends only on  $\lambda_0$ , thus for any given channel the non-dimensional power lost curve (2.4) is solely dependent on the farm's gross drag coefficient,  $\lambda_T$ .

The non-linear equation (2.3) was solved numerically using Runge-Kutta 45 integration using the approximate analytical velocity solution in the appendix (A3) as an initial condition. The model was run until it achieved a steady state. The average power and other information were then calculated from the last full tidal cycle.

### 2.1. Turbine Farm with Gaps

Gaps between turbines will likely be necessary to allow the passage of vessels and marine life along a channel, Fig. 1. GC07 modelled the power produced by turbines in a channel where some flow is allowed to bypass the turbines through gaps. Their model had uniform water depth, uniform steady flow upstream and downstream of the turbines and ignored bottom friction. Their results are expressed in terms of the fraction of the cross-sectional area taken up by the turbines,  $\epsilon$ , and thus, as they note, can be applied either to a single turbine or to many turbines within the same cross-section occupying a total fraction  $\epsilon$ .  $\epsilon$  is effectively the cross-sectional turbine density. They also noted that a farm may consist of multiple rows of turbines and it is assumed that the spacing between rows is large enough to allow the high flow bypassing the turbines in one row to fully mix with the retarded flow passing through the same turbines before encountering the next row.

GC07 showed that the force on the turbines is related to the various velocities in Fig. 1. The force can be expressed as  $F = \rho N_R C_{T1} A_c u^2$ , where  $C_{T1}$  is the drag coefficient for a single row of turbines based on the channel's cross-sectional area and  $N_R$  is the number of rows of turbines in the farm. The total number of turbines in the farm can be written  $N = N_R \epsilon A_c / A_T$ , where  $A_T$  is the blade area of one turbine. From GC07's Eq. 2.8 the drag coefficient for one row of untuned turbines can be written as

$$C_{T1} = \frac{\epsilon}{2} (r_4^2 - r_3^2) \quad (2.5)$$

where  $r_i = u_i/u$  are the ratios of the various velocities near the turbine to the free-stream flow. By using Bernoulli and balancing mass and momentum within control volumes GC07 found an expression for the flow through the gaps between the turbines,  $u_4$  (GC07 Equ. 2.23), which can be rewritten

$$r_4 = \frac{1 - r_3 + \sqrt{\epsilon - 2\epsilon r_3 + (1 - \epsilon + \epsilon^2)r_3^2}}{1 - \epsilon} \quad (2.6)$$

In addition the velocity passing through the turbines relative to the free stream can be expressed in terms of  $r_3$  and  $r_4$  (GC07 Equ. 2.9) as

$$r_1 = \frac{r_3(r_4 + r_3)}{r_4 + 2r_3 - 1} \quad (2.7)$$

GC07 also showed that the power lost by the flow due to the turbines and power available are

$$P_{lost} = Fu = \rho N_R C_{T1} A_c u^3 \quad (2.8)$$

$$P_{avail} = Fu_1 = \rho N_R C_{T1} A_c u^3 r_1 \quad (2.9)$$

The difference between  $P_{lost}$  and  $P_{avail}$  is the energy dissipated as the fast bypassing flow mixes with the slower flow passing through the turbines, with  $r_1$  being the fraction of power lost available for production, GC07. Equations (2.5) and (2.6) show  $C_{T1}$  depends only on  $\epsilon$  and  $r_3$ , and from (2.6) and (2.7).  $r_1$  also depends only on  $\epsilon$  and  $r_3$ . The powers (2.8) and (2.9) are thus functionally expressed as  $P_{lost}(N_R, u, \epsilon, r_3)$  and  $P_{avail}(N_R, u, \epsilon, r_3)$ . Turbine pitch can be adjusted to give particular through-flows measured by  $r_3$ . Thus  $r_3$  can be used as turbine tuning parameter. For an isolated turbine with a constant free-stream flow,  $u$ , Lanchester-Betz found the optimal tuning of  $r_3 = 1/3$ . GC07 found the same optimal tuning,  $r_3 = 1/3$  for a turbine in a channel. However, in a tidal channel driven by a head loss between the ends, the free-stream along-channel flow is not constant but depends on the farm's gross drag coefficient, i.e.  $u(t', \lambda_0 + \lambda_T)$ , where

$$\lambda_T = N_R^* C_{T1}(\epsilon, r_3) \quad (2.10)$$

and the non-dimensional number of rows  $N_R^* = \alpha N_R$ . The dependence of the velocity  $u$  on  $r_3$ , via the drag coefficient  $\lambda_T$ , means the tuning required to maximise both the power lost and available in a tidal channel differs from that given by GC07.

## 2.2. Combined model

Here the GC07 model, which has steady flow and ignores bottom friction, is combined with the tidal channel model of GCO5, which includes bottom friction. As they note in Garrett & Cummins (2008) the differing assumptions may place limits on the applicability of the combined model. Here the combination is rationalised by assuming that the farm takes up only a short section of the channel,  $L_T \ll L$ . Consequently, the force of the turbines dominates bottom friction and flow inertia within a short farm and the headloss across the farm is in a quasi-steady state balance with the velocity. In the broader extent of the channel bottom friction and inertia may still be significant.

To solve the combined model specified values of  $\epsilon$ ,  $r_3$  and  $N_R^*$  are used to calculate  $\lambda_T$ . With  $\lambda_0$  the channel model (2.3) is solved numerically to find the average power lost and available in a single tidal cycle. Peaks in the power lost and available curves were found using numerical searches based on golden section search and parabolic interpolation.

The use of  $r_3$  as the turbine tuning parameter of the combined model warrants some comment. Tuning blade pitch to obtain an optimal flow fraction downstream of the

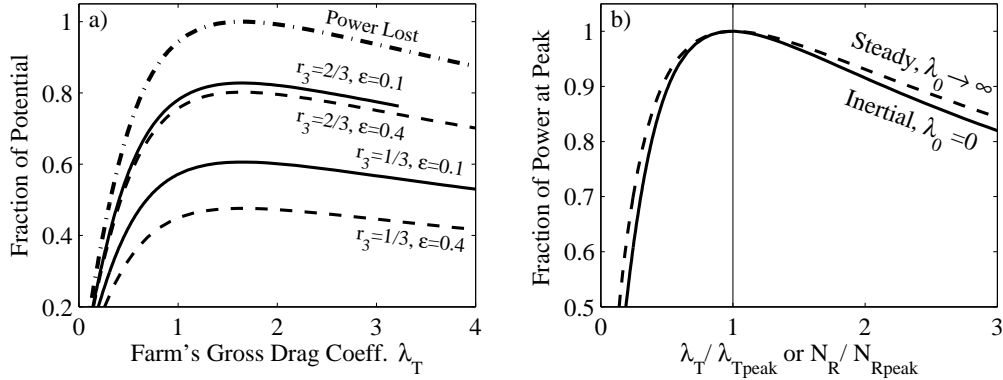


FIGURE 3. a) Curves of power relative to the channel’s potential for a channel with no bottom friction,  $\lambda_0 = 0$ . Chained dashed line is the power lost by the flow due to the turbines. Other curves are power available for generation for different values of  $r_3$  and  $\epsilon$ . Solid lines are for  $\epsilon = 0.1$  and dashed are for  $\epsilon = 0.4$ . b) Power curves of power lost or power available normalised by  $\lambda_{Tpeak}$  and the power at their respective peaks for constant values of  $r_3$  and  $\epsilon$ . Solid line is the inertial limit,  $\lambda_0 = 0$ , and dashed line the steady limit,  $\lambda_0 \rightarrow \infty$ .

turbine,  $r_3$ , is reasonable for an isolated turbine. However, in the confined channel of GC07 and here, the wake size downstream of the turbine depends on the turbine spacing, thus the through flow fraction at the turbine,  $r_1$ , may be a better tuning parameter. The choice of  $r_3$  as the tuning parameter was firstly for easy comparison with the classic and GC07 optimal tunings. Secondly, substituting for  $r_4$ , (2.6), in (2.7) and rearranging would give a complicated expression for  $r_3$  as a function of  $r_1$  and  $\epsilon$ . Thus  $r_3$  was chosen as the tuning parameter partly for mathematical convenience.

The model and its results are presented in terms of a non-dimensional or re-scaled number of rows  $N_R^* = \alpha N_R$ . If this had not been done it would be necessary to explore the effects of the non-dimensional parameter  $\alpha = \frac{a}{\omega^2 L}$ . Thus “non-dimensionalising” the number of rows reduces the number of cases and plots which must be presented. However, the number of rows is an integer and thus for any specific channel  $N_R^*$  is not a continuous variable but takes on discrete values which are integer multiples of  $\alpha$ . If turbines of the same blade area are installed then  $\epsilon$  also only takes on discrete values which are integer multiples of  $A_T/A_c$  as turbines are added to a cross-section.

For a fixed tuning  $r_4$  and  $C_{T1}$  become large as  $\epsilon \rightarrow 1$ . As a result with sufficient rows  $\lambda_T$  (2.10) can be made to exceed  $\lambda_{Tpeak}$  and push the farm beyond the peak in the power curve. Thus for any tuning  $\epsilon$  and  $N_R^*$  can be varied to give a range of farm drag coefficients.

Free surface effects restrict GC07’s model to small Froude numbers,  $u/\sqrt{gh} \ll 1$ . As they note, the enhanced flow through the gaps further restricts the models applicability as  $\epsilon \rightarrow 1$  because  $r_4$  becomes large. Thus the combined model requires  $r_4 a U_0 / \omega \sqrt{gh} \ll 1$ , where  $U_0(\lambda_0 + \lambda_T)$  is from (A 3). This condition varies with turbine tuning and density, as well as the channel’s geometry and tidal forcing. However, the need for navigation will generally restrict  $\epsilon$  to be sufficiently small that this Froude number condition is easily met.

### 3. Power curves and similarity

Fig. 3 gives examples of power curves for a channel. The curves of power lost due to the turbines in Fig. 3a exhibits GC05’s peak at the farm’s optimal drag coefficient,  $\lambda_{Tpeak}$

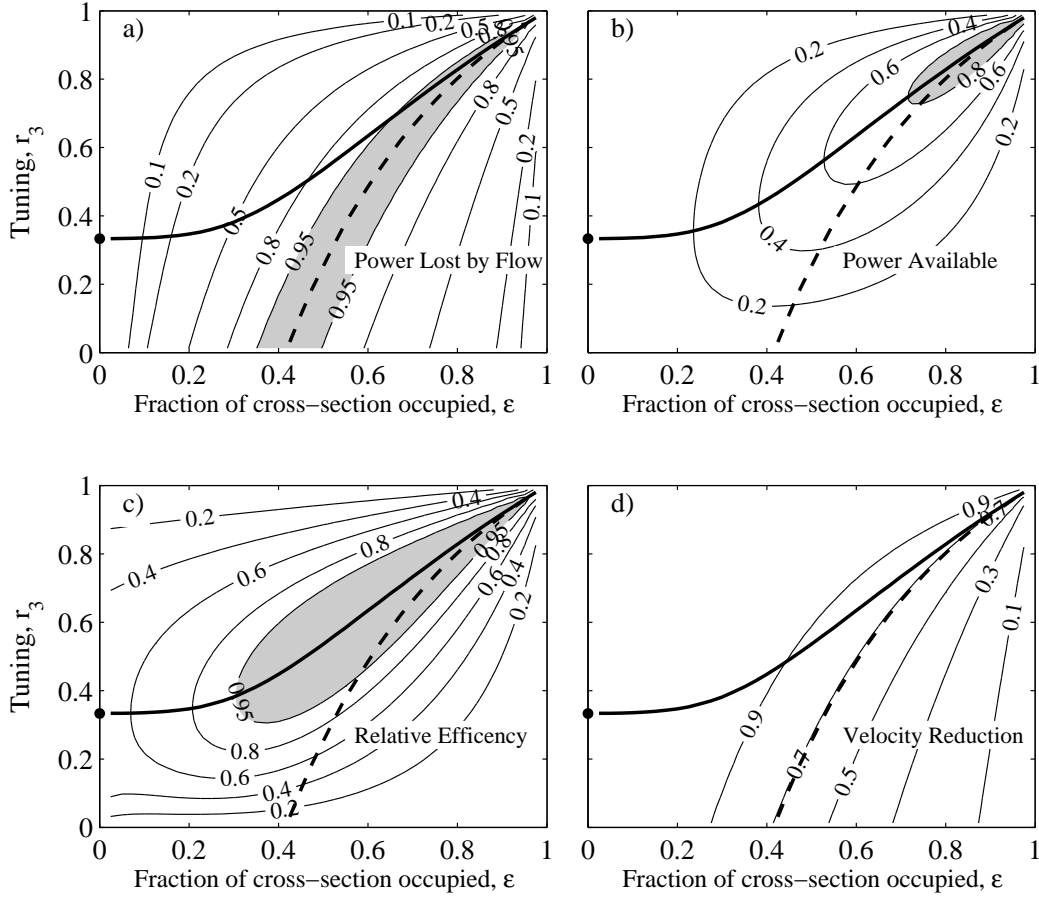


FIGURE 4. Power contours for an inertial channel,  $\lambda_0 = 0$ , for  $N_R^* = 1$ . a) Power lost by flow relative to a channel's potential,  $\bar{P}_{lost}/\bar{P}_{max}$ . b) Fraction of a channel's potential available for production,  $\bar{P}_{avail}/\bar{P}_{max}$ . c) The relative efficiency of the turbines (4.1). d) The reduction in velocity relative to the undisturbed channel. In all plots the thick dashed curve is the tuning,  $r_{3peak}$ , which maximises power lost,  $\bar{P}_{lost}$ , and the thick solid curve the tuning,  $r_{3opt}$ , which maximises power available,  $\bar{P}_{avail}$ . The shaded areas indicated regions with high values.

corresponding to the channel's potential,  $\bar{P}_{max}$ . A channel's potential decreases as the importance of bottom friction,  $\lambda_0$ , increases because bottom friction dissipates energy, which is then not available for power production. Useful results from the approximate analytic solution to GC05's channel model given in the appendix are that

$$\lambda_{Tpeak} \approx \frac{3\pi\sqrt{2}}{8} + 2\lambda_0 \quad (3.1)$$

and that the amplitude of the along channel velocity (A 3) decreases monotonically with increasing farm drag coefficient. A consequence of these results is that increasing the importance of bottom friction,  $\lambda_0$  both reduces a channel's potential and shifts the peak in the power curve to higher  $\lambda_T$  (3.1). Effectively this implies that as bottom friction becomes more important more turbines are required to realise less power when  $r_3$  and  $\epsilon$  are constant.

Scaling the power lost (2.4) by the peak power lost and the farm drag coefficient by

the location of the peak gives normalised power curves

$$\frac{\overline{P}_{lost}}{\overline{P}_{max}} = S \frac{|u'(t', S + S_0)|^3}{|u'(t', 1 + S_0)|^3} \quad (3.2)$$

where  $S = \lambda_T/\lambda_{Tpeak}$  and  $S_0 = \lambda_0/\lambda_{Tpeak}$ . These normalised power curves are thus identical for any given  $\lambda_0$ , i.e. they exhibit similarity. In addition, plotting normalised power curves, Fig. 3b, shows there is little variation between the two extreme dynamical balances of the channel, the inertial limit,  $\lambda_0 = 0$ , and the quasi-steady limit,  $\lambda_0 \rightarrow \infty$ . This demonstrates that the normalised power lost curves exhibit near self-similarity across the full range of dynamical balances, which simplifies the presentation of some later results.

### 3.1. Effects of tuning

The fraction of a channel's potential available varies with  $r_3$  and  $\epsilon$  in Fig. 3a. At  $\epsilon = 0.1$  increasing  $r_3$  from  $1/3$  to  $2/3$  substantially increases the power available, demonstrating that optimal tunings for the tidal channel can differ from GCO7's value of  $1/3$ . In Fig. 3a increasing  $\epsilon$  decreases the power available, as in GC07. However, Fig. 4 (discussed later) demonstrates that whether  $\epsilon$  decreases or increases the power available at a given tuning,  $r_3$ , depends on whether  $\epsilon$  is less than or greater than an optimal  $\epsilon$  value.

Non-dimensionally the power lost curve depends only on  $\lambda_T$  and  $\lambda_0$ . Also the location of its peak,  $\lambda_{Tpeak}$ , is independent of the internal configuration of the turbine farm, but depends only on one channel parameter,  $\lambda_0$  (3.1). Power lost (2.8) and power available (2.9) are both proportional to the force on the turbines. Hence functionally, for constant  $r_3$  and  $\epsilon$ , the power available has the same dependence on  $\lambda_T$  as the power lost, the only difference is power available is reduced by a factor of  $r_1(r_3, \epsilon)$ . Consequently, the peaks in the power available curves for constant  $r_3$  and  $\epsilon$  also occur at  $\lambda_{Tpeak}$ , as demonstrated in Fig. 3a. In addition the power available curves when normalised by  $\lambda_{Tpeak}$  and the power at their respective peaks will also be given by those in Fig. 3b. Thus power available also exhibits near self similarity across the dynamical range when  $r_3$  and  $\epsilon$  are constant. This is a consequence of  $\lambda_T$  being proportional to  $N_R^*$  (2.10), so that  $\lambda_T/\lambda_{Tpeak} = N_R^*/N_{Rpeak}^* = N_R/N_{Rpeak}$  for constant  $r_3$  and  $\epsilon$ , where  $N_{Rpeak}^* = \lambda_{Tpeak}/C_{T1}$ .

## 4. Optimal turbine tunings

### 4.1. Fixed number of rows, $N_R^*$

Fig. 4 shows how tuning and power vary with  $\epsilon$  for a fixed number of turbine rows,  $N_R^* = 1$ . Fig. 4a contours the fraction of a channel's potential lost by the flow. The dashed line,  $r_{3peak}$ , corresponds to the tuning required at the peak in the power curves in Fig. 3a. All points on this curve have that same power lost and the same gross drag coefficient,  $\lambda_{Tpeak}$ . The curve simply gives different combinations of  $\epsilon$  and  $r_3$  which give the same farm drag coefficient (2.10).

There are two optimal tuning curves in Fig. 4. The first  $r_{3peak}$  (thick dashed curve) maximises the power lost by the flow. The second  $r_{3opt}$  (thick solid curve) maximises the power available, which is given in Fig. 4b. These two optimal tuning curves differ, particularly for small  $\epsilon$ . In comparing the two curves in Fig. 4b, by increasing  $r_3$  to move from the dashed curve,  $r_{3peak}$ , around a contour to the solid curve,  $r_{3opt}$ , yields the same power from a smaller  $\epsilon$ , i.e. fewer turbines. The power available at this optimal tuning is maximised at high  $\epsilon$  for  $r_{3opt} \rightarrow 1$ . That is, the turbines occupy almost the entire cross-section and there is no flow reduction downstream of the turbines, as in GC05. At small  $\epsilon$  the optimum tuning tends towards  $r_{3opt} = 1/3$ , the tuning of Lanchester-Betz's

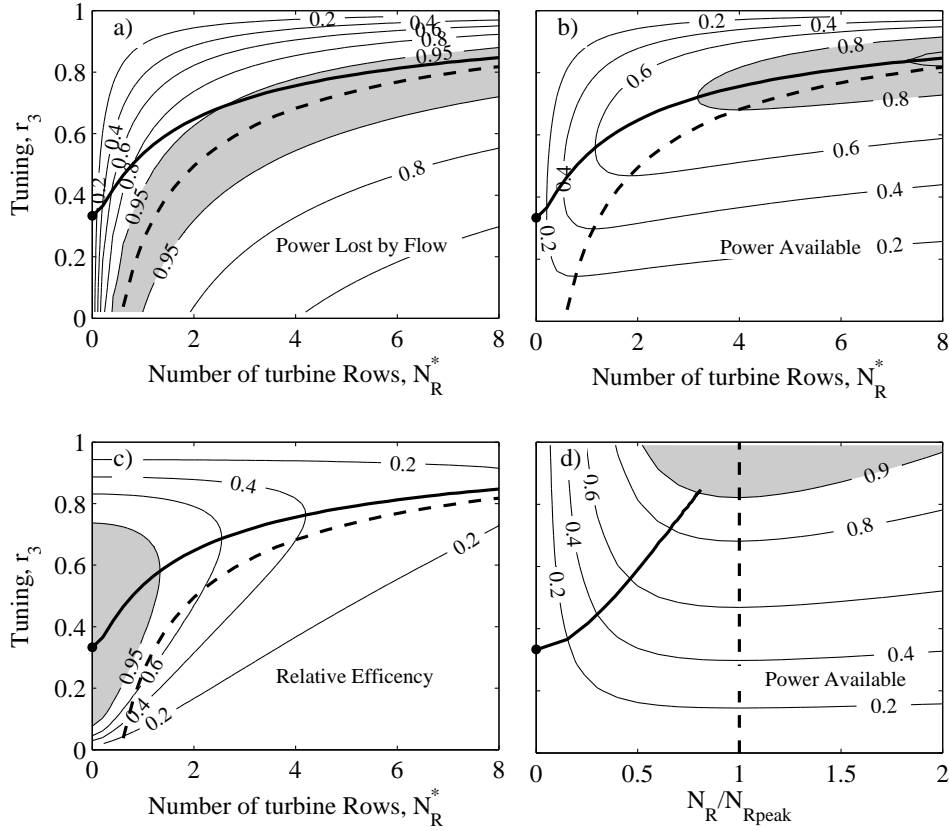


FIGURE 5. Dependence of averaged power or tidal velocity on the number of rows and turbine tuning for an inertial channel,  $\lambda_0 = 0$ , with  $\epsilon = 0.25$ . a) Power lost by flow due to the turbines relative to a channel's potential,  $\bar{P}_{lost}/\bar{P}_{max}$ . b) Fraction of a channel's potential available for production,  $\bar{P}_{avail}/\bar{P}_{max}$ . c) The relative efficiency of the turbines (4.1). The thick dashed line is  $r_{3peak}$  and thick solid line is  $r_{3opt}$ . d) Fraction of power available with x-axis normalised by the number of rows at peak power lost,  $N_{Rpeak}$ . The thick dashed line is  $r_{3peak}$  and thick solid line is  $r_{3opt}$ . Solid dot is  $r_3 = 1/3$ . Shaded regions indicate highest values.

isolated turbine. Figure 4b shows that by adjusting the tuning it is possible to achieve a smooth transition from maximising the power available from an isolated turbine, to almost realising a channel's potential at high  $\epsilon$ .

A measure of the effectiveness or efficiency of each turbine is the power available per turbine normalised by the channel's potential,  $\bar{P}_{avail}/N\bar{P}_{max}$ . Here the relative efficiency will be used, which can be expressed as

$$RE = \frac{\bar{P}_{avail}}{N\bar{P}_{max}} \alpha \frac{A_c}{A_T} = \frac{\bar{P}_{avail}}{\epsilon N_R^* \bar{P}_{max}} \quad (4.1)$$

Fig. 4c gives the relative efficiency for  $N_R^* = 1$ . While the values on the contours of this figure do not have a particular meaning, their relative values show highest efficiencies when optimally tuned to  $r_{3opt}$ . Maximum efficiency requires  $\epsilon$  to be large, i.e. turbines to occupy as much of the cross-section as possible. Interestingly, for this example, when  $\epsilon > 0.3$  the output per turbine is almost constant. Thus the power available for optimally

tuned turbines grows almost linearly with  $\epsilon$  and the number of turbines in the cross-section.

As noted combinations on the dashed line,  $r_{3peak}$ , in Fig. 4 have the same farm drag coefficient, and hence the same velocity, given in Fig. 4d. On the solid  $r_{3opt}$  curve the drag coefficient varies, thus for a given  $\epsilon$  tuning using  $r_{3opt}$  yields more power from stronger along channel flows than using  $r_{3peak}$ . Consequently, a secondary advantage of tuning using  $r_{3opt}$  is less disturbance of the channel's environment by a given number of turbines in the cross-section.

#### 4.2. Fixed cross-sectional density, $\epsilon$

Fig. 5a contours the fraction of a channel's potential available for power production from turbines occupying 25% of the cross-section. Again power lost is maximised on the thick dashed line,  $r_{3peak}$  and power available is maximised along the thick solid line,  $r_{3opt}$ . The same power available on the dashed line can be obtained by moving around a contour in Fig. 5b to the solid line. Thus the same yield from a farm tuned to  $r_{3peak}$  is available from a farm with fewer rows tuned to the higher  $r_{3opt}$ . Viewed from a turbine efficiency perspective, Fig. 5c, efficiency is maximised by a single row of optimally tuned turbines for which  $N_R^* = \alpha$ .

For large optimally tuned farms available power is maximised on the  $r_{3opt}$  curve on the upper right of the figure, demonstrating that even when occupying less than the entire cross-section, it is almost possible to achieve a channel's potential when there are gaps, though this requires a very large number of turbines, i.e.  $N_R, N \rightarrow \infty$ .

Note that as  $\lambda_T \propto N_R$  at constant  $r_3$  and  $\epsilon$  (2.10), the power curves obtained from horizontal slices of both Fig. 5a and b are self similar and look like the curves in Fig. 3b. In addition the near-similarity across the full dynamical range means that the power available contours for an inertial channel in Fig. 5d plotted with a normalised x-axis will be very similar to the contours for a steady state channel,  $\lambda_0 \rightarrow \infty$ . The number of rows required for this normalisation, i.e. the number required to maximise power lost to the turbines, can be obtained from the approximate analytic solution (3.1) giving an expression for the dashed curve in Fig. 5 as

$$N_{Rpeak}^* = \frac{1}{C_{T1}(r_3, \epsilon)} \left( \frac{3\pi\sqrt{2}}{8} + 2\lambda_0 \right) \quad (4.2)$$

Again the number of rows is an integer, thus for a specific channel this expression must take discrete values which are multiples of  $\alpha$ .

#### 4.3. At optimal tuning, $r_{3opt}(N_R^*, \epsilon)$

Fig. 6a shows how optimal tuning  $r_{3opt}$  varies with  $N_R^*$  and  $\epsilon$ , from 1/3 in the lower left for small farms which occupy only a small fraction of the channel cross-section, to near 1 in the upper right for large farms occupying most of the cross-section. The power available in Fig. 6b can approach the channel's potential,  $\bar{P}_{max}$ , for large farms occupying most of the cross-section. The main implication of Fig. 6b is that adding turbines to an optimally tuned farm will always increase the farm's total output, provided  $\epsilon$  remains the same or increases. Also horizontal sections of Fig. 6b demonstrate a 'law of diminishing returns', as the gain per turbine row reduces as an optimally tuned farm grows. Further, sections show that for a given  $\epsilon$  the extra return on each additional turbine is largest at high  $\epsilon$ . As a result, to minimise the number of turbines it is essential to occupy as much of the channel's cross-section as possible. The relative efficiency (4.1) (not shown) emphasises this, by demonstrating the highest return per optimally tuned turbine is at high  $\epsilon$  and small  $N_R^*$ , consistent with Figures 4c and 5c.

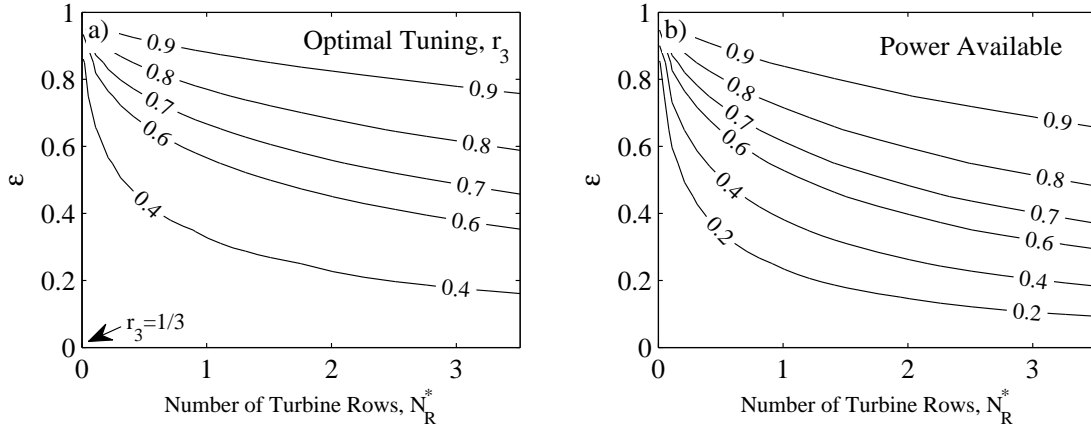


FIGURE 6. Tuning and power at optimal tuning for an inertial channel,  $\lambda_0 = 0$ . a) Optimal tuning,  $r_{3opt}(\epsilon, N_R^*)$ . b) Fraction of a channel's potential available for production,  $\bar{P}_{avail}/\bar{P}_{max}$ .

It should be emphasized that for a specific channel and turbine not all combinations of  $\epsilon$  and  $N_R^*$  in Fig. 6 are possible because the number of rows and the number of turbines in a row are integers. This may require a compromise between the number of turbines in each row and the number of rows to achieve near optimal power availability.

To give some context to the results Table 4.3 gives two hypothetical examples of high flow channels with optimally tuned turbines taking up 25% of the channels' cross-sections. The first a shallow 20 m deep entrance to a large embayment lies near the steady state limit  $\lambda_0 = 5.4$ . The shallow channel has a potential of  $\bar{P}_{max} = 9.0MW$  with 4.8MW of this available from a single row of turbines tuned to  $r_{3opt} = 0.52$  and 8.2MW available from ten rows tuned to  $r_{3opt} = 0.86$  (though ten rows would probably violate the model assumption of widely spaced rows confined to a short section of the shallow channel). The second channel, a 100 m deep tidal strait connecting two water bodies with semi-diurnal tides in anti-phase, lies near the inertial limit,  $\lambda_0 = 0.3$ . The strait's potential is huge,  $\bar{P}_{max} = 5.5GW$ , but only 0.4GW is available from a single row and 2.3GW from ten rows, both at much lower tunings than the shallow channel. In both examples the farm's electricity output will be significantly less than the power available due to the electro-mechanical efficiency of the turbines and drag on the turbines' support structures.

#### 4.4. Effects of dynamical balance

Fig. 7a illustrates the effect dynamical balance has on optimal tuning. This figure shows that, not only as noted earlier does  $r_3 \rightarrow 1/3$  for small  $\epsilon$  and  $N_R$ , but  $r_3$  also tends towards  $1/3$  for steady state channels,  $\lambda_0 \rightarrow \infty$ .

Fig. 7b shows that, in all cases, as the effects of bottom friction become more important,  $\lambda_0 \rightarrow \infty$ , the fraction of a channel's potential that is available for power production decreases. So not only does increasing importance of bottom friction reduce a channel's potential and require more turbines to achieve that potential, bottom friction also reduces the fraction of the potential available for power production. Thus the energy available per square kilometer in deep inertia dominated tidal straits will be relatively much higher than in shallow tidal channels.

Increasing the number of rows in Fig. 7 increases both optimal tunings and the fraction of power available. To realise a large fraction of a channel's potential requires  $\epsilon$  to be large. However if navigation or environmental constraints allow only a small  $\epsilon$ , then a

	A- Shallow Channel	B- Tidal Strait
Depth, $h$	20m	100m
Length, $L$	2km	50km
Width, $W$	500m	10km
Surface Phase Diff./Press. Grad. Phase, $\phi_\eta / \phi_g$	10°/275°	180°/0°
Tidal Amplitude, $\eta_0$ /Headloss amplitude, $\Delta\eta_0$	1.0m/0.17m	0.7m/1.4m
Undisturbed current amplitude	2.7ms <sup>-1</sup>	1.9ms <sup>-1</sup>
$\alpha/\lambda_0$	22/5.4	0.3/0.35
Peak power lost, $\bar{P}_{max}$	9.0MW	5.5GW
One Row - Power available, $\bar{P}_{avail}$	4.8MW	0.4GW
Current amplitude	2.0ms <sup>-1</sup>	1.8ms <sup>-1</sup>
$r_1/r_{3opt}/r_4$	0.72/0.52/1.2	0.55/0.34/1.4
Ten Rows - Power available, $\bar{P}_{avail}$	8.2MW	2.3GW
Current amplitude	1.6ms <sup>-1</sup>	1.6ms <sup>-1</sup>
$r_1/r_{3opt}/r_4$	0.93/0.86/1.1	0.66/0.46/1.3

TABLE 1. Two hypothetical examples of high flow tidal channels with optimally tuned turbines. Both have semi-diurnal tides,  $\epsilon = 0.25$ ,  $\beta = 1$ , and  $C_D = 0.0025$ . For each example  $N_R^*$  is  $\alpha$  times the number of rows.

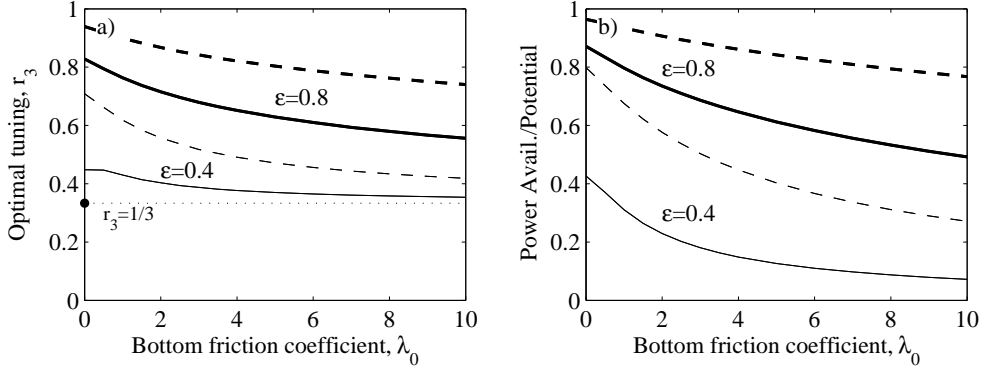


FIGURE 7. Effect of dynamical balance,  $\lambda_0$ , on a) optimal tuning and b) fraction of potential available for power production,  $\bar{P}_{avail}/\bar{P}_{max}$ . Thin lines are for  $\epsilon = 0.4$  and thick lines for  $\epsilon = 0.8$ . Solid lines are for  $N_R^* = 1$  and dashed lines are for  $N_R^* = 5$ . Inertial channels are on the left and quasi-steady state channels are towards the right.

large number of turbine rows are required to achieve a large fraction of potential. Together Figures 7a and 7b demonstrate that in either case, large  $\epsilon$  or large  $N_R^*$ , optimal tunings are well above the 1/3 of an isolated turbine across a realistic dynamical range for high flow tidal channels of  $\lambda_0 = 0.35$  to 5.4 given by the examples in Table 4.3.

## 5. Discussion

A tidal channel's potential depends on properties of the channel, such as  $\lambda_{Tpeak}$  (3.1), and is independent of the farm's internal configuration, i.e.  $N_R^*$ ,  $\epsilon$  and  $r_3$ . For a given along channel flow GC07 found that the useful fraction of the potential, the fraction available, was  $\frac{2}{3(1+\epsilon)}$ . Superficially, their result, that power available decreases as  $\epsilon$  increases, would suggest that farms in tidal channels need to occupy as small a fraction of the channel's cross-section as possible and at most 2/3's of a channel's potential is

available for electricity production. However, for a given headloss the results presented here show that it is possible realise most of a channel's potential if economics permits installation of sufficient optimally tuned turbines. Also, to minimise the required number of turbines, i.e. maximise turbine efficiency, the farm must be configured to occupy the largest fraction of a channel's cross-section permitted by navigational and environmental constraints. Furthermore, for optimally tuned farms, the fluid dynamics yields no optimum number of turbines in Fig. 6b, but efficient optimally tuned farms should grow by densely filling rows first, then adding rows up to the maximum that the economics of the diminishing return on new turbines will allow. The most significant result is that densely packed turbines will need to be tuned for a particular channel and turbine density to maximise a farm's output. Of the two optimal tuning curves  $r_{3peak}$  and  $r_{3opt}$ , the latter can deliver the same power from fewer turbines with less disturbance to along channel flows.

Tunings which maximise power available vary from near  $r_{3opt} = 1/3$ , for small farms occupying only a small fraction of the cross-section, to near  $r_{3opt} = 1$ , for large farms occupying most of the cross-section. Between these two extremes the source of the tidal energy changes smoothly from the flow's kinetic energy, Lanchester-Betz, to headloss across the farm, GC05. Fig. 6a gives the optimal tuning,  $r_{3opt}$ , for farms made up of a grid of turbines, with a non-dimensionalised number of turbines per row,  $\epsilon$ , and a non-dimensionalised number of rows  $N_R^*$ . The figure shows optimal tuning is strongly affected by how turbines are arranged as a grid, as in power available. The tuning is also specific to a particular channel as it varies with its non-dimensional drag coefficient  $\lambda_0 = \alpha C_D L/h$  and  $N_R^* = \alpha N_R$ . As a result, optimal tunings for a particular channel are influenced by its dimensional drag coefficient, length, width, depth, tidal frequency and the amplitude of the tidal forcing.

The model presented is very simple so its ability to predict precise tunings for real farms is limited, however, it demonstrates the necessity of tuning turbines for a particular channel, which has significant implications. One is that there is a strong incentive to construct turbines with the ability to tune blade pitch in real time throughout a tidal cycle in order to maintain the  $r_3$  ratio which maximises their output. However, maintenance costs of difficult to access turbines will encourage the use of mechanically simpler fixed pitched turbines, though this will reduce average turbine output. Fixed tunings will likely be set before turbine installation to achieve the maximum average output for the farm when fully developed. How to optimise fixed tunings will be the subject of a future work. However, the fixed tuning will likely be significantly greater than the  $r_3 = 1/3$  of an isolated turbine and thus fixed pitch turbines will perform sub-optimally until a farm is fully developed.

In the simple geometry of the model flow is assumed uniform across the channel outside of the farm. However, as  $\lambda_0 \propto 1/h$ , the variation of water depth across a channel will result in variation of the dynamical balance (e.g. Vennell (2006)), which in turn will require tunings to vary across the channel, Fig. 7a. Consequently, turbines will need to be individually tuned when water depth varies significantly across a channel. This will also be addressed in a future work.

Turbine flow interaction means that developers using 2D and 3D numerical models to estimate the power available from a proposed turbine farm site will need to include idealised turbines in their models. The necessity of tuning these turbines within efficient densely packed farms for a specific channel and turbine density will require multiple model runs. As a result estimating the power available for a particular site using 2D and 3D numerical models will be an iterative and computationally expensive process.

## Appendix A. Approximate Analytic Solution

Despite a quadratic drag law there is an approximate analytic solution to GC05's model equation (2.3). LeProvost (1991) showed that for a single frequency sinusoidal current,  $u' = U_0 \sin(t' + \phi_g - \phi_u)$ , the drag term  $|u'|u'$  in (2.3) can be expanded to

$$|u'|u' = \frac{8}{3\pi}U_0u' + U_0^2 \sum_{n=1,2,\dots} \frac{8(-1)^{n+1}}{(2n-1)(2n+1)(2n+3)\pi} \sin((2n+1)t' + \phi_g - \phi_u) \quad (\text{A } 1)$$

The terms in the summation are less than 4% of the size of the first term and  $|u'|u'$  is well approximated by the first term alone and with (2.2) becoming

$$U_0 \cos(t' + \phi_g - \phi_u) + \hat{\lambda} U_0^2 \sin(t' + \phi_g - \phi_u) \approx \sin(t' + \phi_g) \quad (\text{A } 2)$$

where  $\hat{\lambda} = \frac{8}{3\pi}(\lambda_0 + \lambda_T)$ . Karsten *et al.* (2008) obtained and solved by an integration technique a similar equation for turbines in a channel connected to a lagoon. The velocity amplitude and phase can be found by expanding (A 2) to give two equations which have solutions

$$U_0 = \frac{\left(\sqrt{4\hat{\lambda}^2 + 1} - 1\right)^{\frac{1}{2}}}{\sqrt{2}\hat{\lambda}} \quad (\text{A } 3)$$

and  $\phi_u = \tan^{-1} \frac{1}{U_0 \hat{\lambda}}$ . The analytic power curves (not shown) are very similar to the numerical solution in Fig. 3, with the analytical solution slightly overestimating the power lost, particularly in inertial channels. Differentiating the analytic power lost gives an expression for the peak's location,  $\lambda_{Tpeak}$ , which is too long to be useful, though there are simple exact peak locations for both the dynamical extremes. Fortunately, a figure in Karsten *et al.* (2008) demonstrates that  $\lambda_{Tpeak}$  is approximately linear between the two dynamical extremes, so that

$$\lambda_{Tpeak} \approx \frac{3\pi\sqrt{2}}{8} + 2\lambda_0 \quad (\text{A } 4)$$

which, considering it is the approximate location of the peak in an approximate solution, agrees well with the numerical peak in Fig. 3a.

## REFERENCES

- BETZ, A . 1920 Das Maximum der theoretisch möglichen Ausnutzung des Windes durch Windmotoren. *Gesamte Turbinenwesen* **Heft 26**.
- BLUNDEN, L. S. & BAHAJ, A. S. 2007 Tidal energy resource assessment for tidal stream generators. *Proc. of the Inst. MECH E Part A J. of Power and Energy* **221**, 137–146(10).
- GARRETT, C. & CUMMINS, P. 2005 The power potential of tidal currents in channels. *Proc. Royal Society A* **461**, 2563–2572.
- GARRETT, C. & CUMMINS, P. 2007 The efficiency of a turbine in a tidal channel. *J. Fluid Mechanics* **588**, 243–251.
- GARRETT, C. & CUMMINS, P. 2008 Limits to tidal current power. *Renewable Energy* **33**, 2485–2490.
- KARSTEN, RH, MCMILLAN, JM, LICKLEY, MJ & HAYNES, RD 2008 Assessment of tidal current energy in the Minas Passage, Bay of Fundy. *Proceedings of the I MECH E Part A Journal of Power and Energy* **222** (5), 493–507.
- LANCHESTER, F. W. 1915 A contribution to the theory of propulsion and the screw propeller. *Trans., Inst. Naval Archit.* **LVII**, 98116.
- LEPROVOST, C. 1991 *Generation of overtides and compound tides, in Tidal Hydrodynamics*, editor B. Parker, pp. 269–296. Wiley.

- VENNELL, R. 1998 Oscillating barotropic currents along short channels. *J. of Physical Oceanography* **28** (8), 1561–1569.
- VENNELL, R. 2006 ADCP measurements of momentum balance and dynamic topography in a constricted tidal channel. *J. of Physical Oceanography* **36** (2), 177–188.